Vehicle System Dynamics
2004, Vol. 42, No. 4, pp. 235–257

Taylor & Francis
Taylor & Francis Group

Performance Benefits in Passive Vehicle Suspensions Employing Inerters[1]

MALCOLM C. SMITH[2] AND FU-CHENG WANG[3]

SUMMARY

A new ideal mechanical one-port network element named the inerter was recently introduced, and shown to be realisable, with the property that the applied force is proportional to the relative acceleration across the element. This paper makes a comparative study of several simple passive suspension struts, each containing at most one damper and inerter as a preliminary investigation into the potential performance advantages of the element. Improved performance for several different measures in a quarter-car model is demonstrated here in comparison with a conventional passive suspension strut. A study of a full-car model is also undertaken where performance improvements are also shown in comparison to conventional passive suspension struts. A prototype inerter has been built and tested. Experimental results are presented which demonstrate a characteristic phase advance property which cannot be achieved with conventional passive struts consisting of springs and dampers only.

1. INTRODUCTION

In [1] an alternative to the traditional electrical-mechanical analogies was proposed in the context of *synthesis* of passive mechanical networks. Specifically, a new two-terminal element called the inerter was introduced, as a substitute for the mass element, with the property that the force across the element is proportional to the *relative* acceleration between the terminals. It was argued in [1] that such an element is necessary for the synthesis of the full class of physically realisable passive mechanical impedances. Indeed, the traditional suspension strut employing springs and dampers only and avoiding the mass element has dynamic characteristics which are greatly limited in comparison. The consequence is that, potentially, there is scope to improve the vehicle dynamics of a passively suspended vehicle by using suspension struts

[1]This work was supported in part by the EPSRC.
[2]Address correspondence to: Malcolm C. Smith, Department of Engineering, University of Cambridge, Cambridge CB2 1PZ, UK. E-mail: mcs@eng.cam.ac.uk
[3]Department of Mechanical Engineering, National Taiwan University, Taipei, Taiwan.

Vehicle System Dynamics
ISSN 0042-3114 print; ISSN 1744-5159 online
http://www.tandf.co.uk/journals
DOI: 10.1080/00423110412331289871

employing inerters as well as springs and dampers. It is the purpose of the present paper to give more detailed consideration to these possible performance benefits using some standard performance measures for quarter-car and full-car vehicle models. In addition, some experimental test results on a prototype inerter will be reported.

2. BACKGROUND ON THE INERTER

The force-current analogy between mechanical and electrical networks has the following correspondences:

force	$\leftrightarrow$	current
velocity	$\leftrightarrow$	voltage
mechanical ground	$\leftrightarrow$	electrical ground
spring	$\leftrightarrow$	inductor
damper	$\leftrightarrow$	resistor.

Additionally, the mass element has always been taken as the analogue of the capacitor, even though it has been appreciated [2, p. 111], [3, p. 10-5] that the mass is strictly analogous only to a capacitor with one terminal connected to ground. This is due to the fact that Newton's Second Law refers the acceleration of the mass to a fixed point in an initial frame, i.e. mechanical ground. The restrictive nature of the mass element in networks has the disadvantage that electrical circuits with ungrounded capacitors do not have a direct spring-mass-damper analogue. This imposes a restriction on the class of passive mechanical impedences which can be physically realised. A further problem is that the suspension strut needs to have small mass compared to that of the vehicle body and wheel hub, which itself imposes further restrictions on the class of mechanical impedances which may be practically realised using the classical spring-mass-damper analogue.

To remedy the situation, a network element called the inerter was introduced in [1] with the following definition. The (ideal) *inerter* is a two-terminal mechanical device with the property that the equal and opposite force F applied at the terminals is proportional to the relative acceleration between the nodes, i.e. $F = b(\dot{v}_2 - \dot{v}_1)$ where v_1, v_2 are the velocities of the two terminals and b is a constant of proportionality called the *inertance* which has units of kilograms. The stored energy in the inerter is equal to $\frac{1}{2}b(v_2 - v_1)^2$.

A variety of different physical realisations of an inerter are possible (see [4]). A simple approach is to take a plunger sliding in a cylinder which drives a flywheel through a rack, pinion and gears (see Figure 1). Such a realisation may be viewed as approximating its mathematical ideal in the same way that real springs, dampers, capacitors, etc. approximate their mathematical ideals.

A table of the circuit symbols of the six basic electrical and mechanical elements, with the inerter replacing the mass, is shown in Figure 2. The symbol chosen for the

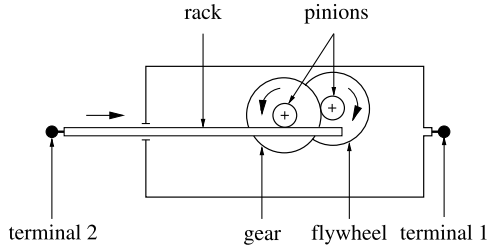

Fig. 1. Schematic of a mechanical model of an inerter.

Mechanical		Electrical	
F — F; υ_2, υ_1	$Y(s) = \frac{k}{s}$	i — i; υ_2, υ_1	$Y(s) = \frac{1}{Ls}$
$\frac{dF}{dt} = k(\upsilon_2 - \upsilon_1)$	spring	$\frac{di}{dt} = \frac{1}{L}(\upsilon_2 - \upsilon_1)$	inductor
F — F; υ_2, υ_1	$Y(s) = bs$	i — i; υ_2, υ_1	$Y(s) = Cs$
$F = b\frac{d(\upsilon_2 - \upsilon_1)}{dt}$	inerter	$i = C\frac{d(\upsilon_2 - \upsilon_1)}{dt}$	capacitor
F — F; υ_2, υ_1	$Y(s) = c$	i — i; υ_2, υ_1	$Y(s) = \frac{1}{R}$
$F = c(\upsilon_2 - \upsilon_1)$	damper	$i = \frac{1}{R}(\upsilon_2 - \upsilon_1)$	resistor

Fig. 2. Circuit symbols and correspondences with defining equations and admittance $Y(s)$.

inerter represents a flywheel. The impedance of a mechanical element, in the force-current analogy, is defined by $Z(s) = \hat{v}(s)/\hat{F}(s)$ (where $\hat{}$ denotes the Laplace transform, v is the relative velocity across the element and F is the force) and the admittance is given by $Y(s) = 1/Z(s)$.

The inerter mechanical element, and the use of the force-current analogy, allows a classical theorem on synthesis of electrical one-ports in terms of resistors, capacitors and inductors to be translated directly into the mechanical context. Although we will not exploit this result directly in the present paper, it is nevertheless useful to cite it. A network is defined to be *passive* if it cannot supply energy to the environment. If a one-port mechanical network has an impedance $Z(s)$ which is real-rational, then it is passive if and only if $Z(s)$ is analytic and $Z(s) + Z(s)^* \geq 0$ in $\mathrm{Re}(s) > 0$ where * denotes complex conjugation. A classical theorem of electrical circuit synthesis, due to Brune, Bott and Duffin, now translates directly over to the following result. See [1] for further details and references as well as a discussion of why this class of impedances is significantly wider than can be obtained using springs and dampers only.

Theorem 1. *Consider any real-rational function $Z(s)$ which is positive real. There exists a one-port mechanical network whose impedance equals $Z(s)$ which consists of a finite interconnection of springs, dampers and inerters.*

3. SUSPENSION STRUTS

We now introduce a few simple networks as candidates for a suspension strut, each of which contains at most one damper and one inerter. While this does not exploit the full class of impedances/admittances of Theorem 1, it nevertheless provides a number of new possibilities to investigate which are relatively simple to realise in practice.

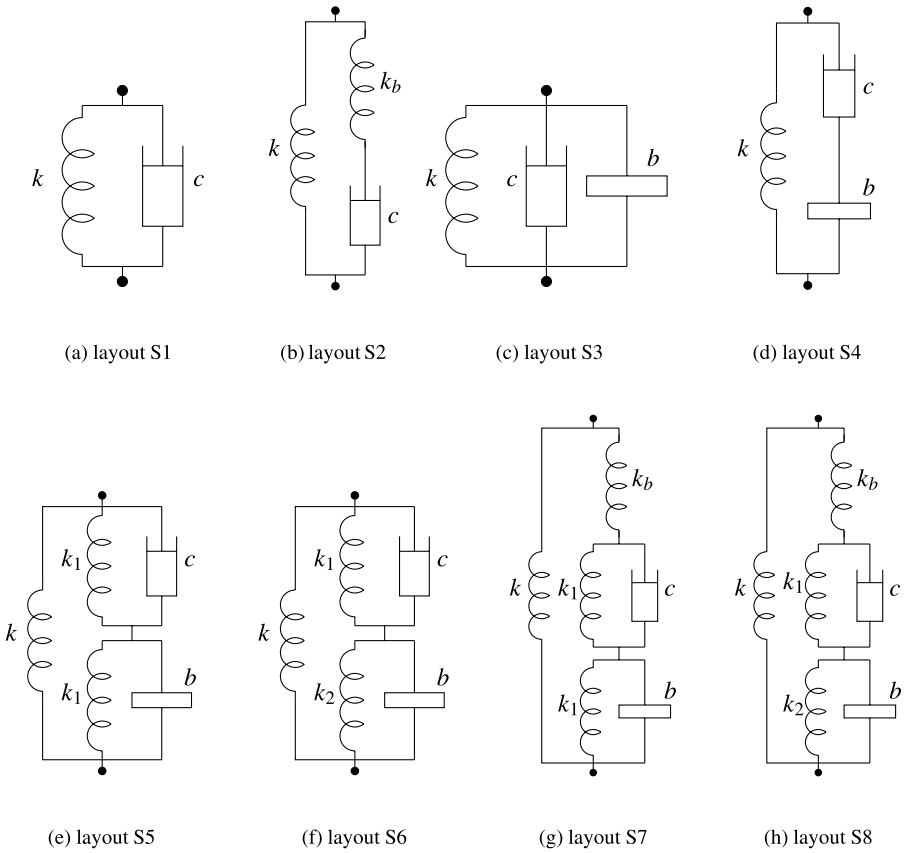

(a) layout S1 (b) layout S2 (c) layout S3 (d) layout S4

(e) layout S5 (f) layout S6 (g) layout S7 (h) layout S8

Fig. 3. The eight suspension layouts.

Figure 3a shows the conventional parallel spring-damper arrangement. In Figure 3b there is a relaxation spring k_b in series with the damper. Figures 3c and 3d show a parallel spring-damper augmented by an inerter in parallel or in series with the damper. When the spring stiffness k is fixed it often proves relatively straightforward to optimise over the two remaining parameters b and c in these configurations.

The series arrangement of Figure 3d has a potential disadvantage in that the node between the damper and inerter has an absolute location which is indeterminate in the steady-state. This could give rise to drift of the damper and/or inerter to the limit of travel in the course of operation. To remedy this the arrangement of Figure 3e is proposed with a pair of springs of stiffness k_1, which we call centring springs, which may be preloaded against each other. Figure 3f is similar but allows for unequal springs k_1 and k_2. Figures 3h and 3g differ from Figures 3f and 3e by having an additional relaxation spring k_b.

The mechanical admittance $Y(s)$ for two of these layouts (layout S3 and S7) is now given for illustration:

$$Y_3(s) = \frac{k}{s} + c + bs \qquad \text{and} \qquad Y_7(s) = \frac{k}{s} + \frac{1}{\frac{s}{k_b} + \frac{s}{cs+k_1} + \frac{s}{bs^2+k_1}}.$$

4. THE QUARTER-CAR MODEL

An elementary model to consider the theory of suspension systems is the quarter-car of Figure 4 consisting of the sprung mass m_s, the unsprung mass m_u and a tyre with spring stiffness k_t. The *suspension strut* provides an equal and opposite force on the sprung and unsprung masses and is assumed here to be a passive mechanical

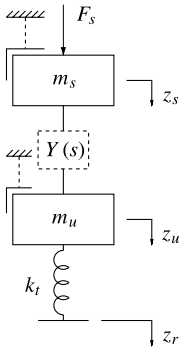

Fig. 4. Quarter-car vehicle model.

admittance $Y(s)$ which has negligible mass. The equations of motion in the Laplace transformed domain are:

$$m_s s^2 \hat{z}_s = \hat{F}_s - sY(s)(\hat{z}_s - \hat{z}_u), \tag{1}$$

$$m_u s^2 \hat{z}_u = sY(s)(\hat{z}_s - \hat{z}_u) + k_t(\hat{z}_r - \hat{z}_u). \tag{2}$$

In this paper we will fix the parameters of the quarter-car model as follows: $m_s = 250\,\text{kg}$, $m_u = 35\,\text{kg}$, $k_t = 150\,\text{kN/m}$.

4.1. Performance Measures

There are a number of practical design requirements for a suspension system such as passenger comfort, handling, tyre normal loads, limits on suspension travel etc. which require careful optimisation. In the simplified quarter-car model, these can be translated approximately into specifications on the disturbance responses from F_s and z_r to z_s and z_u. We now introduce several basic measures.

We first consider road disturbances z_r. Following [5] a time-varying displacement $z(t)$ is derived from traversing a rigid road profile at velocity V. Further, let $z(t)$ have the form $z'(x)$ where x is the distance in the direction of motion. Thus $z(t) = z'(Vt)$. Moreover, the corresponding spectral densities are related by

$$S^z(f) = \frac{1}{V} S^{z'}(n)$$

where f is frequency in cycles/second, n is the wavenumber in cycles/metre and $f = nV$. Now consider an output variable $y(t)$ which is related to $z(t)$ by the transfer function $H(s)$. Then the expectation of $y^2(t)$ is given by:

$$\begin{aligned} E[y^2(t)] &= \int_{-\infty}^{\infty} |H(j2\pi f)|^2 S^z(f)\, df \\ &= \frac{1}{2\pi} \int_{-\infty}^{\infty} |H(j\omega)|^2 \frac{1}{V} S^{z'}(n(\omega))\, d\omega. \end{aligned}$$

Here we will use the following spectrum [5]

$$S^{z'}(n) = \kappa |n|^{-2} \ (\text{m}^3/\text{cycle})$$

where κ is a road roughness parameter. We take $V = 25\,\text{m s}^{-1}$ and $\kappa = 5 \times 10^{-7}\,\text{m}^3\,\text{cycle}^{-1}$. The r.m.s. *body vertical acceleration* parameter J_1 (ride comfort) is defined by

$$\begin{aligned} J_1 &= \left(\frac{1}{2\pi V} \int_{-\infty}^{\infty} \left| T_{\hat{z}_r \to \ddot{\hat{z}}_s}(j\omega) \right|^2 \frac{\kappa}{n(\omega)^2}\, d\omega \right)^{1/2} \\ &= 2\pi (V\kappa)^{1/2} \left\| s T_{\hat{z}_r \to \hat{z}_s} \right\|_2 \end{aligned} \tag{3}$$

where $T_{\hat{x}\to\hat{y}}$ denotes the transfer function from $\hat{x}$ to $\hat{y}$ and $\|f(j\omega)\|_2 = (\frac{1}{2\pi}\int_{-\infty}^{\infty}|f(j\omega)|^2\,d\omega)^{1/2}$ is the standard $\mathcal{H}_2$-norm. Similarly the r.m.s. *dynamic tyre load* parameter J_3 is defined by

$$J_3 = 2\pi(V\kappa)^{1/2}\left\|\frac{1}{s}T_{\hat{z}_r\to k_t(\hat{z}_u-\hat{z}_r)}\right\|_2.$$

Another factor to be considered is the ability of the suspension to withstand loads on the sprung mass, e.g. those induced by braking, accelerating and cornering. Following [6] we make use of the following measure for this purpose:

$$J_5 = \|T_{\hat{F}_s\to\hat{z}_s}\|_\infty$$

where $\|\cdot\|_\infty$ represents the $\mathcal{H}_\infty$-norm, which is the supremum of the modulus over all frequency. Note that this norm equals the maximal power transfer for square integrable signals, so it is a measure of dynamic load carrying.

4.2. Optimisation of Individual Performance Measures

Although suspension design will usually involve a trade-off between various performance measures, it is useful to consider first how much improvement can be obtained in individual performance measures for various different struts.

Our approach is to fix the static stiffness of the suspension strut and then optimise over the remaining parameters. This will be done for a range of static stiffness settings from $k = 10$ kN/m to $k = 120$ kN/m. This covers a range from softly sprung passenger cars through sports cars and heavy goods vehicles up to racing cars. It should be noted that the static stiffness in S1 to S4 of Figure 3 is equal to k but not for the other four struts. For example, for layout S8 the static stiffness is equal to: $k + (k_b^{-1} + k_1^{-1} + k_2^{-1})^{-1}$.

4.2.1. Optimisation of J_1 (Ride Quality)

The results of optimisation are shown in Figures 5 and 6. It was found that the relaxation spring k_b did not prove helpful to reduce J_1. This left five of the eight struts in Figure 3 to be considered. Optimisation for layouts S1, S3, and S4 appears to be convex in the free parameters. Both the parallel (S3) and series (S4) arrangements gave improvements over the conventional strut (S1) for the full range of static stiffness with S4 giving the biggest improvement for stiff suspensions. It should be noted that the parallel arrangement gives lower values of inertance than the series arrangement. For example, at the midrange value of $k = 60$ kN/m we have $b = 31.27$ kg and $b = 333.3$ kg, respectively.

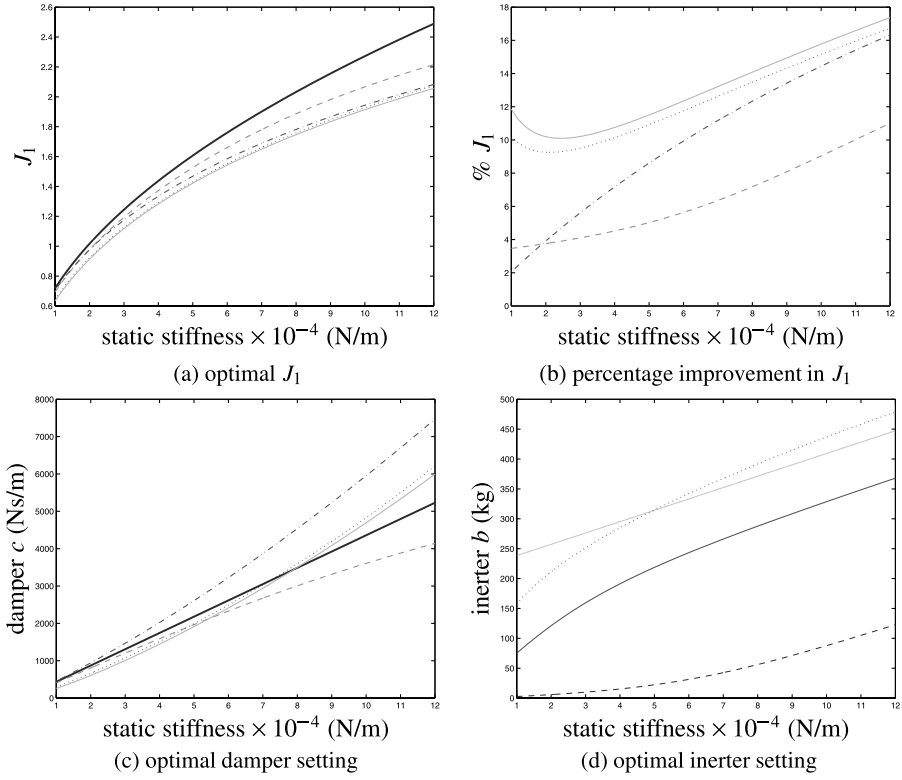

Fig. 5. The optimisation of J_1 on: layout S1 (bold), layout S3 (dashed), layout S4 (dot-dashed), layout S5 (dotted) and layout S6 (solid).

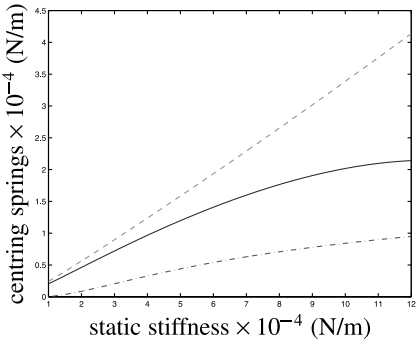

Fig. 6. The optimisation of J_1: k_1 in layout S5 (solid), k_1 in layout S6 (dashed) and k_2 in layout S6 (dot-dashed).

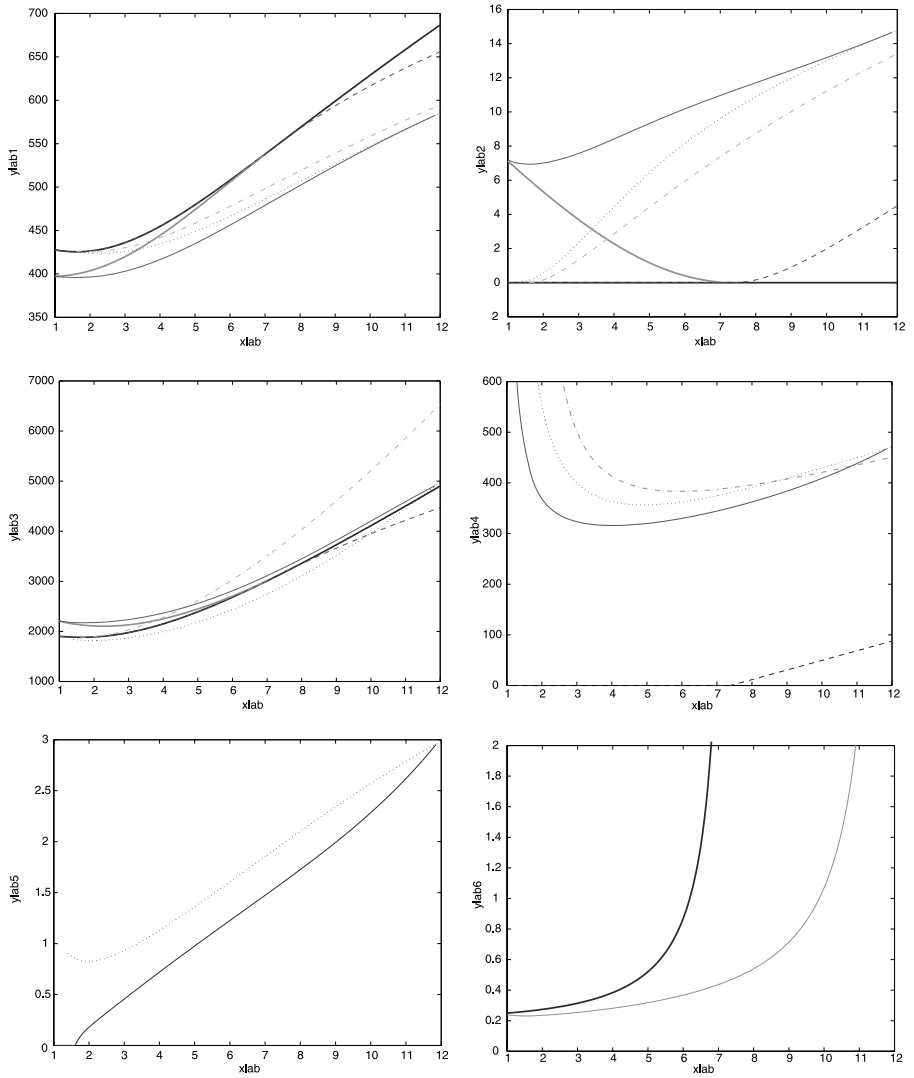

Fig. 7. The optimisation of J_3 on: layout S1 and S2 (bold), layout S3 (dashed), layout S4 (dot-dashed), layout S5 (dotted) and layout S7 (solid).

For layouts S5 and S6, the optimisation problem appears no longer to be convex in the parameters. The Nelder–Mead simplex method was used for various starting points. Solutions were found which gave a clear improvement

on the series arrangement S4 particularly for softer suspensions. For the arrangement S6 the improvement was at least 10% across the whole stiffness range. For much of the range, k_1 and k_2 were about 1/3 and 1/12 of the static stiffness, respectively.

4.2.2. Optimisation of J_3 (Tyre Loads)

The results of optimisation are shown in Figure 7. Here it was found that the relaxation spring k_b helped to reduce J_3 for lower values of static stiffness. Indeed, the conventional strut S2 is a noticeable improvement on S1 for softer suspensions. Again optimisation for layouts S1, S2, S3, and S4 appears to be convex in the free parameters. The results show an improvement in J_3 with parallel (S3) and series (S4) arrangements if the static stiffness is large enough, with the series arrangement again giving the biggest improvement.

For layouts S5 and S6, the optimisation problem appears no longer to be convex in the parameters. The Nelder–Mead simplex method was again used for various starting points. As before, the use of centring springs in layouts S5 and S6 gave further improvements over the ordinary series arrangements S4. The use of a relaxation spring k_b in S7 was needed to extend the benefits to softer suspensions.

4.2.3. Optimisation of J_5 (Dynamic Load Carrying)

In Figure 8 the optimisation of J_5 is illustrated for S1, S3 and S4 only. There is a theoretical minimum for J_5 equal to the d.c. gain of the transfer function $T_{\dot{F}_s \to \dot{z}_s}$, which is equal to $(k_0^{-1} + k_t^{-1})^{-1}$ where k_0 is equal to the static stiffness of the suspension. This can be achieved using layout S1 for k less than about 68 kN/m. The upper and lower bounds for c to achieve this are shown in Figure 8c. Using layout S3, the theoretical minimum for J_5 can be achieved for k up to about 100 kN/m. The upper and lower bounds for c and b to achieve this are shown in Figures 8c and 8d. Using layout S4, the theoretical minimum for J_5 is not achievable beyond $k \approx 68$ kN/m. In contrast to J_1 and J_3 it appears to be the parallel arrangement (S3) which is more effective than the series one (S4) to reduce J_5.

4.3. Multi-Objective Optimisation

In suspension design it is usually necessary to consider several performance objectives. It is interesting to ask if the inerter can give improvements to more than one objective simultaneously. In this section, we will consider J_1 and J_5 together.

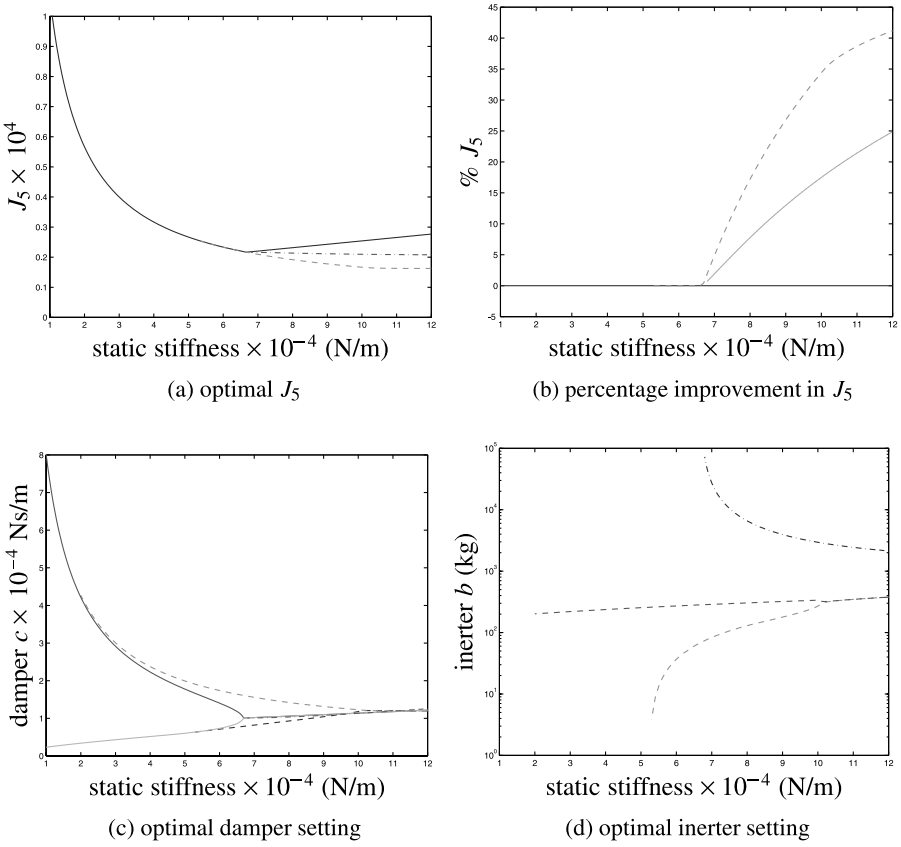

Fig. 8. The optimisation of J_5 on: layout S1 (solid), layout S3 (dashed), layout S4 (dot-dashed).

Our approach is to work with a combined performance index as follows:

$$J := \alpha J_1/J_{1,0} + (1-\alpha)J_5/J_{5,0},$$

for $0 \leq \alpha \leq 1$, with $J_{1,0} = 1.76$ and $J_{5,0} = 2.3333 \times 10^{-5}$ which are the optimal values for suspension layout S1. The optimisation results for a static stiffness of $k = 60$ kN/m are illustrated in Figure 9. Firstly, it is noted that for each layout the optimisation appears to be Pareto optimal, i.e. it is not possible to improve them together in a given layout, as shown in Figure 9. Secondly, the use of inerters (layouts S3, S4) gives the possibility of improving J_1 and J_5 together in comparison to layout S1.

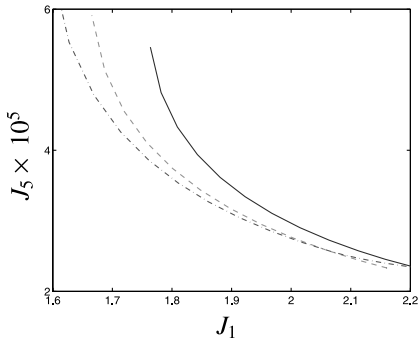

Fig. 9. The optimisation of J_1 and J_5 together: layout S1 (solid), layout S3 (dashed) and layout S4 (dot-dashed).

5. THE FULL-CAR MODEL

We now consider the full-car model as shown in Figure 10. The following parameters taken from [7] will be used: $m_s = 1600\,\text{kg}$, $I_\theta = 1000\,\text{kg m}^2$, $I_\phi = 450\,\text{kg m}^2$,

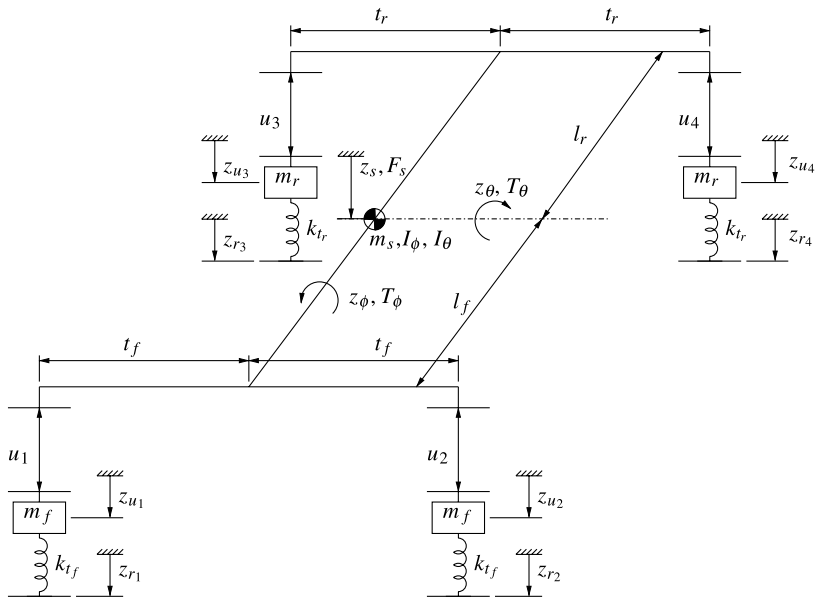

Fig. 10. The full-car model.

$t_f = 0.75\,\text{m}$, $t_r = 0.75\,\text{m}$, $l_f = 1.15\,\text{m}$, $l_r = 1.35\,\text{m}$, $m_f = 50\,\text{kg}$, $m_r = 50\,\text{kg}$, $k_{t_f} = 250\,\text{kN/m}$, $k_{t_r} = 250\,\text{kN/m}$.

5.1. Road Disturbances

Our general approach to obtain a full-car stochastic performance measure is based on a method of Heath [8]. This section briefly describes our approach to obtain a simple approximation to this measure which can be evaluated in Matlab.

Consider a full-car model moving at a speed of V with road inputs $z_{r_i} = x_i$, for $i = 1, \ldots, 4$ and with $c = 2t_f = 2t_r$ and $L = l_f + l_r$. Suppose we select a set of outputs determined by $\hat{y} = P(s)\hat{x}$, where $\hat{x} = (\hat{x}_1, \hat{x}_2, \hat{x}_3, \hat{x}_4)^t$. If the vehicle is running in a straight line, that is, the road inputs to the rear wheels are regarded as time delays of the inputs to the front wheels, then

$$\begin{pmatrix} \hat{x}_3 \\ \hat{x}_4 \end{pmatrix} = e^{-sT} \begin{pmatrix} \hat{x}_1 \\ \hat{x}_2 \end{pmatrix},$$

where $T = L/V$. Hence the system outputs satisfy

$$\hat{y}(s) = P(s) \begin{pmatrix} I \\ e^{-sT} I \end{pmatrix} \hat{u} =: H(s)\hat{u}, \tag{4}$$

where $\hat{u} = (\hat{x}_1, \hat{x}_2)^t$. If x is WSS (Wide Sense Stationary), then the power spectral density functions $S_{uu}(j\omega)$ and $S_{yy}(j\omega)$ are related by [9, Sec. 10-3]

$$S_{yy}(j\omega) = H(j\omega) S_{uu}(j\omega) H^*(j\omega). \tag{5}$$

By definition the autocorrelation of the (front) road surface is given by:

$$\begin{aligned} R_{uu}(\tau) &= E(u(t+\tau)u(t)^t) \\ &= E \begin{pmatrix} x_1(t+\tau)x_1(t) & x_1(t+\tau)x_2(t) \\ x_2(t+\tau)x_1(t) & x_2(t+\tau)x_2(t) \end{pmatrix}. \end{aligned} \tag{6}$$

If we suppose the road surface is *isotropic*, then $E(x_1(t+\tau)x_1(t)) = E(x_2(t+\tau)x_2(t))$ and $E(x_1(t+\tau)x_2(t)) = E(x_2(t+\tau)x_1(t))$. Let $R_D(\tau) = E(x_1(t+\tau)x_1(t))$ and $R_X(\tau) = E(x_1(t+\tau)x_2(t))$. An auto-spectrum S_D and a cross-spectrum S_X are defined as the Fourier transforms of the correlations $R_D(\tau)$ and $R_X(\tau)$ respectively. Then the power spectral density of the road inputs becomes

$$\begin{aligned} S_{uu}(j\omega) &= \int R_{uu}(\tau) e^{-j\omega\tau} d\tau \\ &= \begin{pmatrix} S_D & S_X \\ S_X & S_D \end{pmatrix}. \end{aligned} \tag{7}$$

The relation between S_D and S_X is given by a normalised, real cross-spectrum $g(j\omega)$ in [5, 8] as

$$g(j\omega) = \frac{S_X(j\omega)}{S_D(j\omega)}.$$

Next suppose we can find a spectral factorisation of the following matrix:

$$\begin{bmatrix} 1 & g \\ g & 1 \end{bmatrix} = MM^*. \tag{8}$$

Then the power spectrum of the road inputs becomes

$$S_{uu} = WMM^*W^*, \tag{9}$$

where

$$W = W^* = \begin{bmatrix} \sqrt{S_D} & 0 \\ 0 & \sqrt{S_D} \end{bmatrix}.$$

From Equations (5) and (4) we then obtain

$$S_{yy} = HS_{uu}H^* = HWMM^*W^*H^*.$$

Then we define the performance measure of interest as

$$\begin{aligned} y_{\text{rms}} &= \left(\frac{1}{2\pi} \int \text{trace}(S_{yy}) d\omega \right)^{1/2} \\ &= \left(\frac{1}{2\pi} \int \text{trace}([HWM][HWM]^*) d\omega \right)^{1/2} \\ &= \left\| P \begin{pmatrix} I \\ e^{-sT} I \end{pmatrix} WM \right\|_2. \end{aligned} \tag{10}$$

As in Section 4 we consider a time-varying displacement $x(t)$ derived from traversing a rigid road profile at velocity V. Further, let $x(t)$ have the form $x'(z)$ where z is the distance in the direction of motion. Thus $x(t) = x'(Vt)$. Moreover, the corresponding spectral densities are related by [5]

$$S^x(f) = \frac{1}{V} S^{x'}(n),$$

where $f = nV$. A similar relationship holds for the cross-spectrum. Here we will use the following spectrum

$$S^{x'} = \frac{\kappa}{n^2}, \ (\text{m}^3/\text{cycle})$$

where κ is a road roughness parameter. We take $\kappa = 5 \times 10^7\,\mathrm{m}^3\,\mathrm{cycle}^{-1}$. We therefore obtain

$$S_D(j\omega) = \frac{\kappa V (2\pi)^2}{\omega^2}. \tag{11}$$

In [8] the following expression is obtained for the normalised cross-spectrum (in terms of displacement)

$$\frac{2|\pi cn|}{\Gamma(1)} \mathrm{K}_1(|2\pi cn|),$$

where K_1 is the modified Bessel function of the second kind of order 1, and Γ is the gamma function. We therefore see that

$$\begin{aligned} g(j\omega) &= \frac{|c\omega|}{\Gamma(1)V} \mathrm{K}_1(|c\omega/V|) \\ &= \lambda\omega \mathrm{K}_1(\lambda\omega) =: g_\lambda(j\omega), \end{aligned} \tag{12}$$

where $\lambda = c/V$. We note that $g(j\omega)$ is a real function of ω and is irrational.

To calculate the performance measure numerically the time-delay e^{-sT} was approximated as follows:

$$e^{-sT} \simeq \frac{\Pi_1^n(2n/T - s)}{\Pi_1^n(2n/T + s)},$$

with $n = 6$. In addition the following approximation was used in the matrix W in (10):

$$\frac{1}{s} \simeq \frac{\tau}{\tau s + 1},$$

where $\tau = 10^2$. This makes little difference in the calculation value of y_{rms} because, in cases of interest, $P(s)$ has zeros at the origin. To deal with $g(j\omega)$ a particular value $\lambda = 0.05$ was selected and $\sqrt{g_{0.05}(j\omega)}$ was evaluated frequency by frequency. The command *fitmag* in Matlab was used to give an approximation: $g_{0.05}(j\omega) \simeq hh^* =: \bar{g}(j\omega)$ which allows the approximation $g_\lambda(j\omega) \simeq \bar{g}(j\frac{\lambda}{0.05}\omega)$ to be used. A spectral factorisation was then calculated

$$M_{0.05} = \begin{bmatrix} \bar{M}_{11} & \bar{M}_{12} \\ \bar{M}_{12} & \bar{M}_{11} \end{bmatrix} = \left[\begin{array}{c|c} A & B \\ \hline C & D \end{array}\right], \tag{13}$$

where

$$\bar{M}_{11} = \frac{(s + 75.30 \pm 116.35j)(s + 53.96 \pm 42.74j)(s + 23.05)(s + 7.05)}{(s + 75.29 \pm 116.36j)(s + 54.03 \pm 43.26j)(s + 28.43)(s + 8.00)},$$

$$\bar{M}_{12} = \frac{14.3836(s + 75.88 \pm 117.70)(s + 63.80 \pm 39.97j)(s + 9.26)}{(s + 75.29 \pm 116.36j)(s + 54.03 \pm 43.26j)(s + 28.43)(s + 8.00)}.$$

Then, the approximation for any speed V and wheel track c was taken to be:

$$M \simeq \left[\begin{array}{c|c} \alpha A & \sqrt{\alpha} B \\ \hline \sqrt{\alpha} C & I \end{array}\right], \tag{14}$$

where $\alpha = \frac{V}{20c}$.

5.2. Optimisation of Full-Car Performance Measures

In this section, we shall compare the performance improvement of the full-car model with inerters in the suspension struts. Our approach is to optimise J_1 and J_3 (defined below) over choices of the front and rear dampers c_f and c_r for the conventional suspension (layout S1), or over choices of the front and rear inerters and dampers b_f, b_r, c_f and c_r for layout S3 at each corner, and including centring springs k_{1_f} and k_{1_r} for layout S5. We will take a fixed static stiffness for each suspension strut equal to 100 kN/m. We will assume the vehicle has a forward velocity $V = 25$ m/sec (90 km/h).

5.2.1. The Optimisation of J_1 (Ride Quality)

We will compute the r.m.s. body acceleration parameter $J_1 = y_{\text{rms}}$ where $P = T_{\hat{\boldsymbol{u}} \to \hat{\boldsymbol{y}}}$ with $u = [z_{r_1}, z_{r_2}, z_{r_3}, z_{r_4}]'$ and $y = [\ddot{z}_s, \ddot{z}_\theta, \ddot{z}_\phi]'$. From Equation (10) we can calculate and compare the performance of the full-car model with various layouts. The results are illustrated in Table 1. It is noted that for layout S1 the optimisation of J_1 over c_f and c_r appears to be convex, as shown in Figure 11. But the optimisations for layouts S3, S5 do not necessarily find a global optimum. Similar to the quarter-car case, we observe an improvement in both parallel and series arrangements.

5.2.2. The Optimisation of J_3 (Tyre Loads)

We now compute the r.m.s. dynamic tyre load parameter $J_3 = y_{\text{rms}}$ from (10) where $P = T_{\hat{\boldsymbol{u}} \to \hat{\boldsymbol{y}}}$ with $u = [z_{r_1}, z_{r_2}, z_{r_3}, z_{r_4}]'$ and $y = [k_{t_f}(z_{u_1} - z_{r_1}), k_{t_f}(z_{u_2} - z_{r_2}), k_{t_r}(z_{u_3} - z_{r_3}), k_{t_r}(z_{u_4} - z_{r_4})]'$. The results are illustrated in Table 2. Again it is noted

Table 1. Performance index J_1 with various layouts at each wheel station, percentage improvement and parameter settings (k's are in kN/m, c's are in kNs/m, b's are in kg).

Layout	Optimal J_1	Parameter settings
Conventional (layout S1)	2.7358	$c_f = 2.98$, $c_r = 3.70$
Parallel inerter (layout S3)	2.5122 (8.17% improvement)	$b_f = 31.07$, $b_r = 44.23$ $c_f = 2.32$, $c_r = 3.16$
Series inerter with centring springs (layout S5)	2.4823 (9.26% improvement)	$b_f = 332.82$, $b_r = 374.03$ $c_f = 3.24$, $c_r = 3.94$ $k_{1_f} = 7.85$, $k_{1_r} = 14.10$

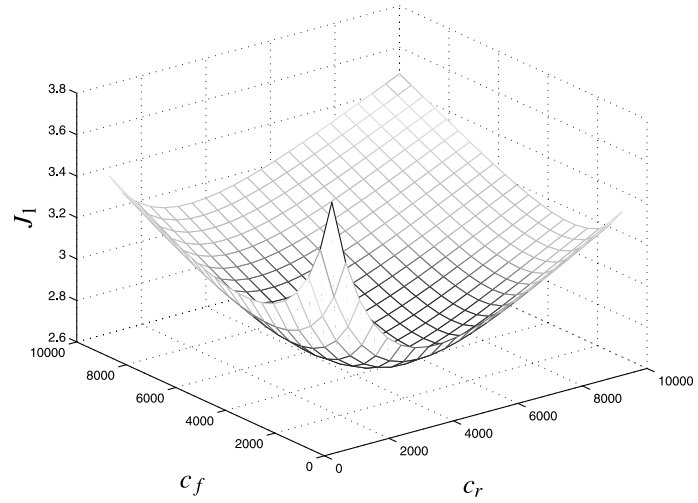

Fig. 11. The optimisation of J_1 over c_f and c_r for layout S1.

Table 2. Performance index J_3 ($\times 10^{-3}$) with various layouts at each wheel station, percentage improvement and parameter settings (k's are in kN/m, c's are in kNs/m, b's are in kg).

Layout	Optimal J_3	Parameter settings
Conventional (layout S1)	1.6288	$c_f = 3.82$, $c_r = 3.85$
Parallel inerter (layout S3)	1.6288 (0% improvement)	$b_f = 0$, $b_r = 0$ $c_f = 3.82$, $c_r = 3.85$
Series inerter with centring springs (layout S5)	1.5224 (6.53% improvement)	$b_f = 710.74$, $b_r = 418.42$ $c_f = 3.16$, $c_r = 3.71$ $k_{1_f} = 35.01$, $k_{1_r} = 25.10$

that for layout S1 the optimisation of J_3 over c_f and c_r appears to be convex. But the optimisations for layouts S3, S5 do not necessarily find a global optimum. Similar to the quarter-car case, at some values of static stiffness an improvement is obtained with the series arrangement but not with the parallel.

6. EXPERIMENTAL RESULTS

A variety of different embodiments of an inerter are possible (see [4]). A prototype of rack and pinion design has been built and tested at Cambridge University Engineering

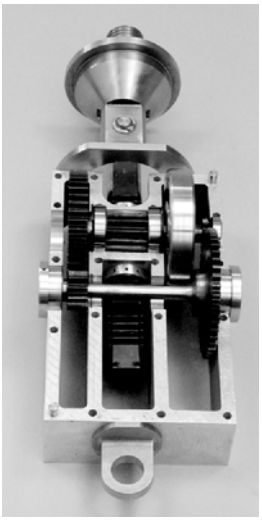

Fig. 12. Prototype inerter.

Department (see Figure 12). There are two gearing stages with combined ratio of 19.54:1. The flywheel has a mass of 0.225 kg and the total *inertance* of the device is approximately 726 kg. A clutch safety mechanism is integrated into the flywheel to prevent loads in excess of 1.5 kN being delivered to the piston. The device has a stroke of about 80 mm.

The inerter was tested in a series arrangement with centring springs as shown in Figure 13 using the Cambridge University mechanics laboratory Schenck hydraulic ram. A series of single sinewave excitations was applied at a set of discrete frequencies from 0.05 to 20 Hz. Three signals were measured: the total force in the strut, the total displacement, and the relative displacement across the inerter. Gains and phase shifts for the different signal paths were calculated frequency by frequency [10].

The ideal linear model of the strut is shown in Figure 14. The admittance Y of the strut is given by the following expression:

$$Y = \frac{(bs^2 + k)(cs + k_1)}{s(bs^2 + cs + k + k_1)}. \tag{15}$$

It is noted that there is a zero at the frequency $\omega = \sqrt{k/b}$. As in Figure 14, let D_c and D_b represent the displacements of the damper and inerter respectively, and let

Fig. 13. Inerter in series with damper with centring springs.

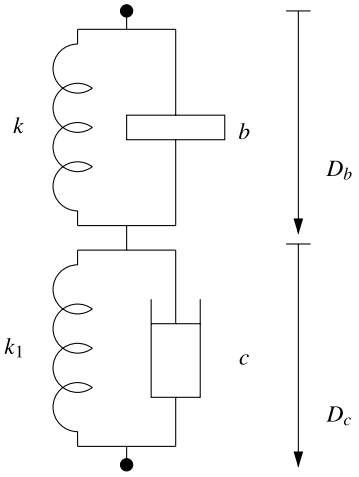

Fig. 14. Mechanical network circuit diagram for inerter-damper series connection with centring springs.

the total strut displacement be $D = D_b + D_c$. Then the following transfer functions can be derived:

$$\hat{\boldsymbol{D}}_c(s) = \frac{bs^2 + k}{bs^2 + cs + k_1 + k}\hat{\boldsymbol{D}}(s), \tag{16}$$

$$\hat{\boldsymbol{D}}_b(s) = \frac{cs + k_1}{bs^2 + cs + k_1 + k}\hat{\boldsymbol{D}}(s). \tag{17}$$

Ideal frequency responses were calculated for each of the transfer functions in Equations (15), (16) and (17) with the following parameters, which were estimated by measurements on the individual physical components: $k = 5.632\,\text{kN/m}$, $k_1 = 9.132\,\text{kN/m}$, $c = 4.8\,\text{kNs/m}$, $b = 726\,\text{kg}$. In addition, stiction nonlinearities were incorporated into the model in parallel with the inerter and damper by adding a force $20\,\text{sign}(\dot{\boldsymbol{D}}_b)$ to the inerter force, and a force $30\,\text{sign}(\dot{\boldsymbol{D}}_c)$ to the damper force, corresponding to physically measured stiction forces. Sinewave tests on a nonlinear simulation model were carried out at the same set of frequencies as the practical experiments. The resulting time response data were analysed in a similar way to produce a corresponding set of frequency responses for comparison. The Bode plots corresponding to each of the transfer functions in

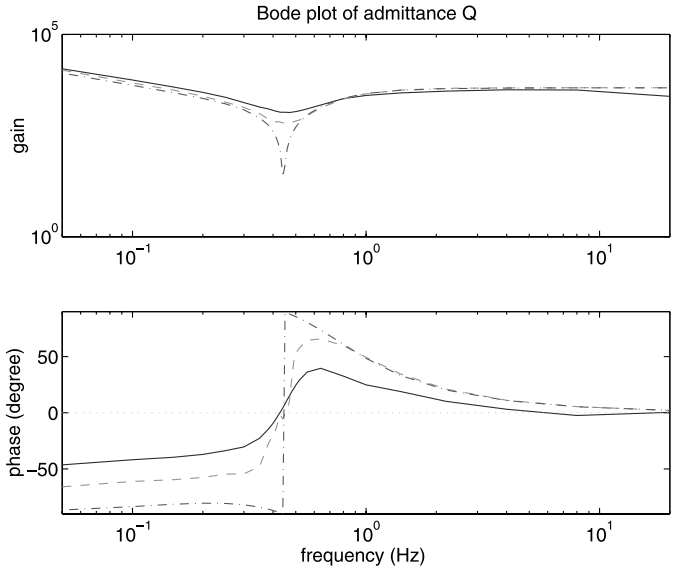

Fig. 15. Bode plot of the admittance $Y(s)$: linear model (dash-dotted), nonlinear simulation with friction (dashed), experimental data (solid).

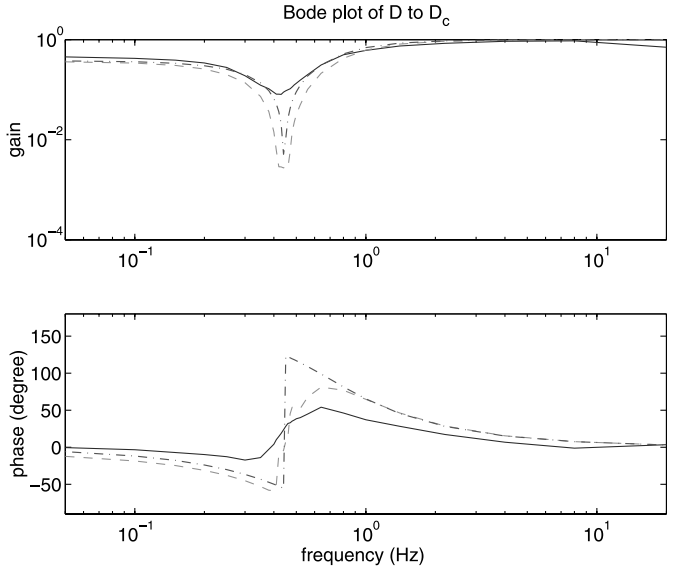

Fig. 16. Bode plot of transfer-function $\hat{\boldsymbol{D}}_c(s)/\hat{\boldsymbol{D}}(s)$: linear model (dash-dotted), nonlinear simulation with friction (dashed), experimental data (solid).

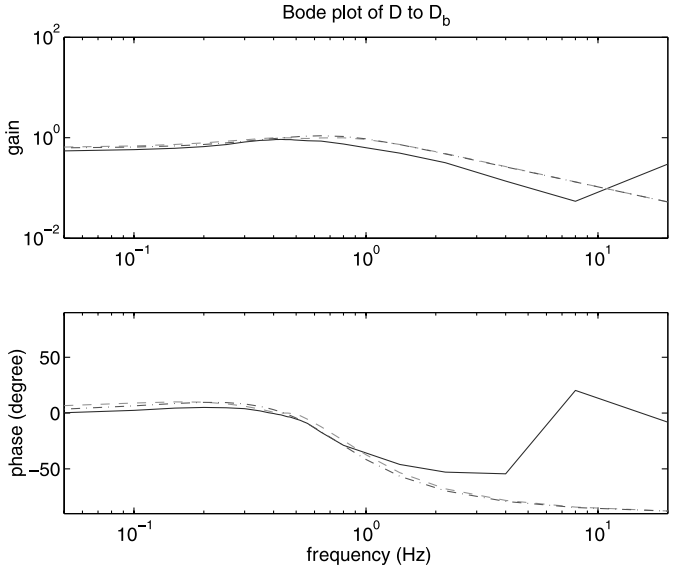

Fig. 17. Bode plot of transfer-function $\hat{\boldsymbol{D}}_b(s)/\hat{\boldsymbol{D}}(s)$: linear model (dash-dotted), nonlinear simulation with friction (dashed), experimental data (solid).

Equations (15), (16) and (17), for (i) ideal linear, (ii) nonlinear simulation and (iii) experimental results, are shown in Figures 15, 16 and 17. It was felt that the agreement between simulation and experiment was relatively good – in particular the phase advance was clearly in evidence in the admittance Y – and optimisation of parameters to get a closer fit between simulation and experiment was not attempted.

7. CONCLUSIONS

This paper represents a preliminary optimisation study of the possible benefits of the inerter in vehicle suspension systems. For some relatively simple struts it was shown that improvements could be obtained in a quarter-car vehicle model across a wide range of static suspensions stiffnesses. Improvements of about 10% or greater were shown for measures of ride, tyre normal load and handling. For certain combinations of these measures, good simultaneous improvement was obtained. Improvements were also shown for a full-car model. A prototype inerter was built and tested in a series arrangement with centring springs and shown to exhibit the expected phase advance property.

ACKNOWLEDGEMENTS

We are most grateful to Samuel Lesley, Peter Long, Neil Houghton, John Beavis, Barry Puddifoot and Alistair Ross for their work in the design and manufacture of the inerter prototype. We would also like to thank David Cebon for making the Vehicle Dynamics Group's hydraulic ram available to us, and to Richard Roebuck for his assistance in the experiments.

REFERENCES

1. Smith, M.: Synthesis of Mechanical Networks: The Inerter. *IEEE Transactions on Automatic Control* 47 (2002), pp. 1648–1662.
2. Shearer, J., Murphy, A. and Richardson, H.: *Introduction to System Dynamics*, Addison-Wesley, 1967.
3. Hixson, E.: *Mechanical Impedance, Shock and Vibration Handbook, 2nd edition*, C.M. Harris, C.E. Crede (Eds.), McGraw-Hill, 1976.
4. Smith, M.: Force-Controlling Mechanical Device, Patent Pending, Intl. App. No. PCT/GB02/03056, Priority Date: 4 July 2001.
5. Robson, J.: Road Surface Description and Vehicle Response. *Int. J. Vehicle Des.* 1(1) (1979), pp. 25–35.
6. Smith, M. and Walker, G.: A Mechanical Network Approach to Performance Capabilities of Passive Suspensions. In: *Proceedings of the Workshop on Modelling and Control of Mechanical Systems*, Imperial College, London, 17–20 June 1997, pp. 103–117, Imperial College Press, London, 1997.

7. Smith, M. and Wang, F.-C.: Controller Parameterization for Disturbance Response Decoupling: Application to Vehicle Active Suspension Control. *IEEE Trans. on Contr. Syst. Tech.* 10 (2002), pp. 393–407.
8. Heath, A.: Application of the Isotropic Road Roughness Assumption. *J. Sound Vib.* 115(1) (1987), pp. 131–144.
9. Papoulis, A.: *Probability, Random Variables, and Stochastic Process*, McGraw-Hill, 1991.
10. Ljung, L.: *System Identification, Theory for the User*, Prentice-Hall, 1987.